AIP | Review of Scientific Instruments

Design, construction, and performance of a real-time holographic refractometry prototype for liquid analysis

E. A. Barbosa, D. M. Silva, A. O. Preto, and R. Verzini

Citation: Rev. Sci. Instrum. **82**, 013103 (2011); doi: 10.1063/1.3523049
View online: http://dx.doi.org/10.1063/1.3523049
View Table of Contents: http://rsi.aip.org/resource/1/RSINAK/v82/i1
Published by the AIP Publishing LLC.

Design, construction, and performance of a real-time holographic refractometry prototype for liquid analysis

E. A. Barbosa,[a] D. M. Silva, A. O. Preto, and R. Verzini
Laboratório de Óptica Aplicada, Faculdade de Tecnologia de São Paulo, CEETEPS-UNESP, Pça Cel Fernando Prestes, 30, 01124–060 São Paulo, Brazil

(Received 30 August 2010; accepted 9 November 2010; published online 21 January 2011)

The development and the performance of a portable holographic refractometer prototype for liquid measurement employing multimode diode lasers with emission centered at 662 nm as light sources is reported. Due to the multiwavelength character of the holographic recording, a synthetic wavelength was generated, and the diffracted wave intensity was thus modulated as a function of the optical path difference between the reference and the object beams. The transparent test cell containing the liquid was placed at the reference-beam arm of the optical setup, while the contour interferogram generated on the holographic image of a flat object was used for fringe counting. A change ΔL on the liquid column length is proportional to the Δp running fringes on the object image, and from this relation the refractive index of the test liquid was obtained. The holograms were recorded on a photorefractive $Bi_{12}TiO_{20}$ crystal whether using a single multimode diode laser or by combining two diode lasers. In the latter configuration the synthetic wavelength can be varied in order to enhance the measurement sensitivity and/or to allow the analysis of turbid liquids. The size of the whole prototype is 54 $\times$ 22 $\times$ 14 cm^3. The refractive indexes of ethanol/water mixtures with different concentrations were measured, as well as the NaCl concentrations in aqueous solutions were determined upon comparison with an empirical curve. In both cases the results were compared with the ones obtained through an Abbe refractometer. © *2011 American Institute of Physics*. [doi:10.1063/1.3523049]

I. INTRODUCTION

Refractive index measurement has become an important tool in a large variety of measurements with applications in fields ranging from agriculture to industry, including also scientific, technological, and medical applications. In biological sciences, refractometry was employed to determine salinity levels due to total plasma protein (TPP) in fish blood samples[1] and in avian species,[2] to study the molecular basis of virus entry by analyzing the interactions between cellular receptors of herpes virus and the viral glycoproteins in a molecular level,[3] to evaluate the purity and the quality of antimalarial drugs,[4] to rapidly measure glucose concentration in blood,[5,6] and to diagnose and evaluate the evolution of tumors in breast tissues.[7] By performing refractive index measurements, the study of bubble flow,[8] as well as the characterization of optical,[9] polymeric,[10,11] and chemical[12,13] materials can be carried out. For such a large variety of applications many refractometry devices were proposed and developed concerning the particularities of each application. Although the probably most popular devices are the Abbe refractometers[14] employed in agriculture and wine production in order to evaluate sugar concentration in fruit juices and wine, a wide range of refractometers based on several optical phenomena have been reported and produced in the last years in order to fulfill the increasing demand for precise, reproducible, simple, and reliable measurements. The literature has been reporting an increasing number of refractometry techniques based on interference and diffraction, due to the typically high precision and accuracy of the measurements obtained through these phenomena.[15–19] Among these diffractive and interferometric methods, the holographic ones present interesting characteristics since they usually provide two-dimensional interferograms and thus allow for whole-field measurements.[20,21]

A novel refractometry concept was recently proposed and demonstrated by obtaining fringe-modulated holographic images of prism-shaped transparent media using a $Bi_{12}TiO_{20}$ (BTO) crystal and a multimode laser.[22] By measuring the spatial period of the resulting interference pattern, the refractive indexes of prism-shaped amorphous samples were determined. Despite the very good results and the quite satisfactory performance of that optical setup, it presented some drawbacks. For instance, since the measurement precision increases with a larger optical path inside the test cell, the volume character of the cell required a somewhat large amount of material to be analyzed in order to increase the precision, which constitutes itself a limitation of the technique. Moreover, this can make the uniform temperature distribution in the sample and its monitoring somewhat difficult to achieve. A large test cell brings also other difficulties such as the need of large-area, high-quality glass walls with very small thickness irregularities and high flatnesses, thus increasing the cost of the whole apparatus.

Based on the same refractometry principle, this work proposes a novel optical setup, and the construction of a portable apparatus aiming easier, more precise, and more reproducible measurements in real-life environments. In the experimental arrangement the object is a flat metallic plate tilted with respect to the BTO front face at an arbitrary angle.

[a]Electronic mail: ebarbosa@fatecsp.br.

The multiwavelength emission of the diode laser generates straight and parallel contour fringes on the holographic object according to a synthetic wavelength λ_S.[23,24] The reference beam in turn passes through a glass cell filled with the liquid to be analyzed with a moveable reflector inside. As the mirror is translated, the liquid column length is varied, thus changing the optical path of the reference beam. This phase shift onto the reference beam makes the contour fringes run on the object surface so that the mirror translation for a given fringe displacement is inversely proportional to the refractive index of the liquid. The rectangular cross section and the reduced dimensions of the cell require smaller amounts of liquid for considerably larger optical paths of the laser beam if compared to the refractometer using prism-shaped cells. The collimated, small-diameter beam passing through the cell assures a high intensity reference beam at the BTO crystal even if relatively turbid liquids are analyzed.

In order to evaluate the sensitivity of the device to small refractive index variations, we analyzed a solution of water with different ethanol concentrations. Moreover, the concentrations of NaCl in water saline solutions were determined by comparing the measured refractive indexes with a previously obtained curve. In both cases the results were compared with values obtained through a commercial Abbe refractometer. We studied also the performance of the system for turbid liquid measurements; the refractive index of a turbid melon juice was made by using a two-laser holographic setup in order to significantly decrease the synthetic wavelength. This enabled the analysis of much smaller amounts of liquid through smaller mirror displacements. In addition, the scalableness of the measurement precision was analyzed upon using different reflector geometries inside the test cell.

II. MULTIWAVELENGTH PHOTOREFRACTIVE HOLOGRAPHIC RECORDING AND REFRACTIVE INDEX MEASUREMENT

In this section a brief review of multiwavelength holographic recording and readout in sillenite crystals is presented in order to obtain an expression for the refractive index based on the optical setup geometry. At the holographic medium the reference and signal beams originated from a laser emitting simultaneously N longitudinal modes interfere. If the whole recording process occurs by self-diffraction in the pure diffusion regime, the intensity of the diffracted wave is given as a function of the reference wave intensity I_R by[22]

$$I_D \propto \left\{ \frac{\sin[N\Delta k(\Gamma_S - \Gamma_R)/2]}{\sin[\Delta k(\Gamma_S - \Gamma_R)/2]} \right\}^2 I_R, \tag{1}$$

where Δk is the wavenumber gap between two adjacent modes, and Γ_S and Γ_R are the optical paths of the object and the reference beams at the photorefractive crystal, respectively. Equation (1) shows clearly that the holographic image of the object appears modulated by a contour interference pattern. From this equation one obtains the optical path variation $\Delta\Gamma_R$ introduced onto the reference wave, which is able to shift the interference pattern by one period:

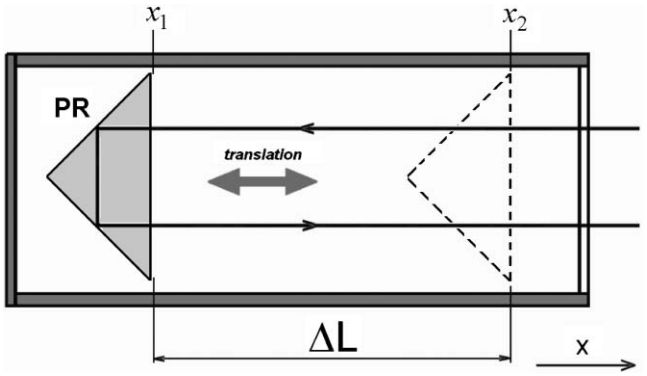

FIG. 1. 90°-prism retroreflector PR in test cell.

$$\Delta\Gamma_R = \frac{2\pi}{\Delta k} = \frac{\lambda^2}{\Delta\lambda} \equiv \lambda_S, \tag{2}$$

where $\Delta\lambda$ is the wavelength difference between two consecutive laser modes and λ is the central emission wavelength of the laser.

In order to introduce an optical path variation into the reference beam a glass test cell with a 90°-prism retroreflector PR inside was employed, so that when the liquid is introduced into the cell the PR becomes immersed. Figure 1 shows the light beam traveling through the fluid and being reflected by the PR so that its total optical path through a liquid column of length L and refractive index n is $\Gamma_R = 2nL$. After exiting the test cell the beam impinges the BTO crystal, thus constituting the reference beam. Consider a given configuration 1 with a point A on the object holographic image illuminated by a bright fringe and the PR at a position x_1 (Fig. 1). For such a configuration one gets from Eq. (1) the relation $\Gamma_S - \Gamma_{R1} = 2\pi q/\Delta k$, where Γ_S is the optical path of the object beam through A, Γ_{R1} is the reference beam optical path at the position x_1, and q is an integer. In a configuration 2 the prism PR is displaced by ΔL to a position x_2 until p bright fringes pass through A, so that one obtains, correspondingly, $\Gamma_S - \Gamma_{R2} = 2\pi(p+q)/\Delta k$. Since the total change in the reference beam optical path is $\Gamma_{R2} - \Gamma_{R1} = 2n(x_2 - x_1) = 2n\Delta L$, from the relations above and from Eq. (2), the refractive index of the liquid can be written as

$$n = \frac{\lambda_S p}{2\Delta L}, \tag{3}$$

Two-laser holography—when a two-diode laser configuration is employed, the laser beams are coupled and superimposed with the help of a beam splitter (BS) and are tuned in order to provide smaller synthetic wavelengths.[25] In this case, the refractive index is obtained from Eq. (3) also, with λ_S given by $\lambda_S = 2\lambda_1\lambda_2/(\lambda_1 - \lambda_2)$, where λ_1 and λ_2 are the central wavelengths of the lasers. This setup is useful for turbid liquid media analysis and in cases for which only small amounts of liquid are available.

III. EXPERIMENTS AND RESULTS

In the optical setup a 40-mW diode laser (Laserline, model L40) centered at 662 nm was used as light source and

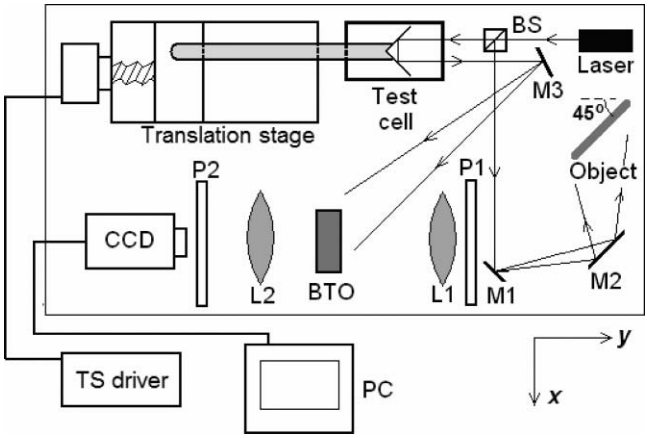

FIG. 2. Optical setup for the holographic refractometer: BTO, $Bi_{12}TiO_{20}$ crystal; BS, beam splitter; M1 and M2, mirrors; P1 and P2, polarizers; L1 to L3, lenses; translation stage TS driver, CCD camera and PC computer for image acquisition.

a BTO crystal cut in the [110]-transverse electrooptic configuration was the storage medium. Through this crystal orientation one exploits the anisotropic diffraction properties of the sillenite-family crystals, which makes the transmitted and the diffracted beams to be orthogonally polarized at the crystal output.[26] An analyzer behind the BTO crystal blocks the transmitted wave, thus enabling the detection of the diffracted one only and enhancing the signal-to-noise ratio of the resulting images. The light emerging from the cell is the reference beam after being reflected by mirror M3, while mirror M2 illuminates the object. A 16-mm focal length objective (lens L1 in Fig. 2) images the object onto the BTO crystal thus constituting the object beam, and a microscope objective (lens L2) forms the holographic image of the metallic plate onto the CCD target. This plate is ~45° tilted with respect to the BTO front face in order to generate straight and parallel contour fringes according to Eq. (1). Since the illuminated area on the object is relatively small (~1 cm^2), the total intensity of the waves impinging the BTO is high enough to provide relatively short hologram buildup times of about 5 s. The optical scheme for two-wave mixing holography is depicted in Fig. 2.

The setup is mounted on a breadboard of anodized aluminum. Crossed steel bars placed under the 54 × 22-cm^2 breadboard allow the whole structure to prevent the optical setup against external perturbations. The short hologram buildup also contributes for the interferogram visualization even in moderately noisy environments. In order to avoid instabilities generated by air drift the arrangement is protected by an opaque case made of black acrylic resin. Due to this structure stable holographic images can be obtained without the need of placing the apparatus on massive optical tables with vibration damping systems. Pictures of the whole interferometer (with open cap) are shown in Figs. 3(a) and 3(b). The cell with dimensions 50 × 80 × 15 mm^3 ($x \times y \times z$) is mounted on a robust translation stage, and its upper part is open. Through its aluminum base the cell can be efficiently

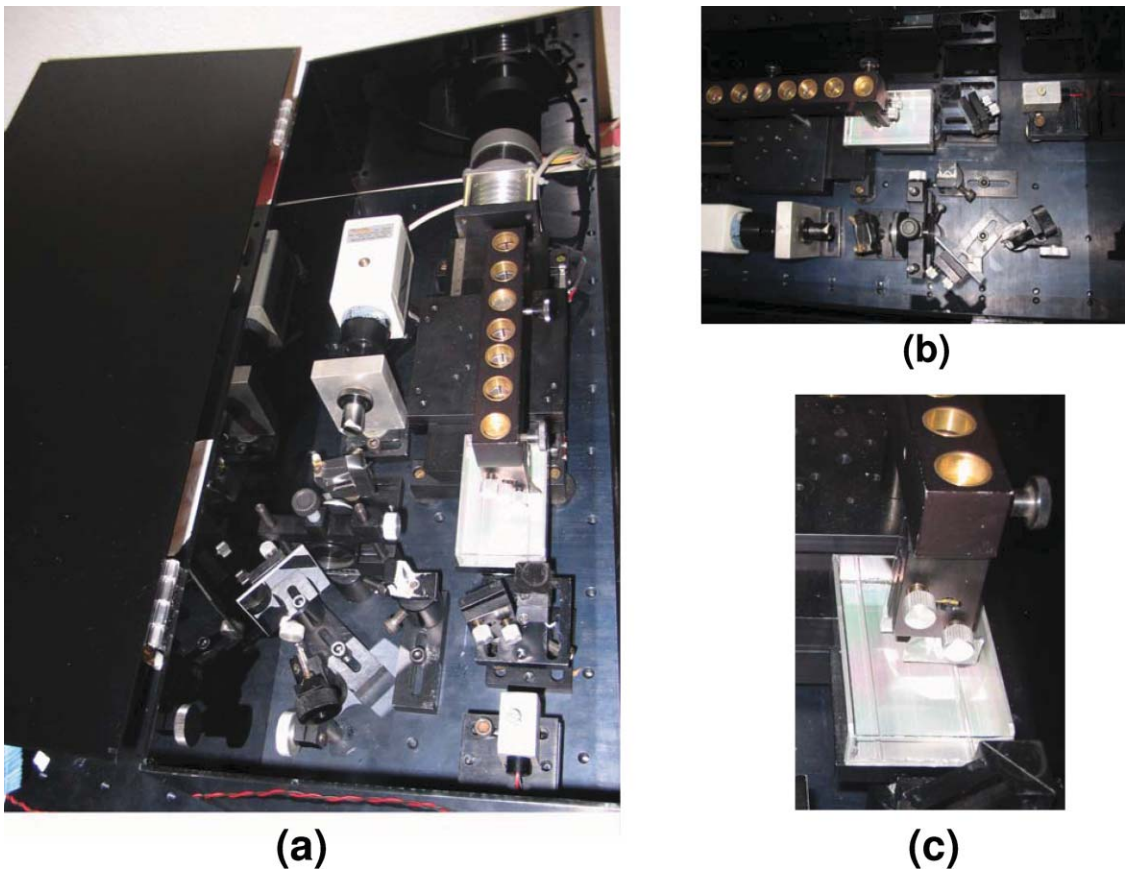

FIG. 3. (Color online) (a) and (b) Pictures of the refractometer prototype; (c) PR mount and test cell.

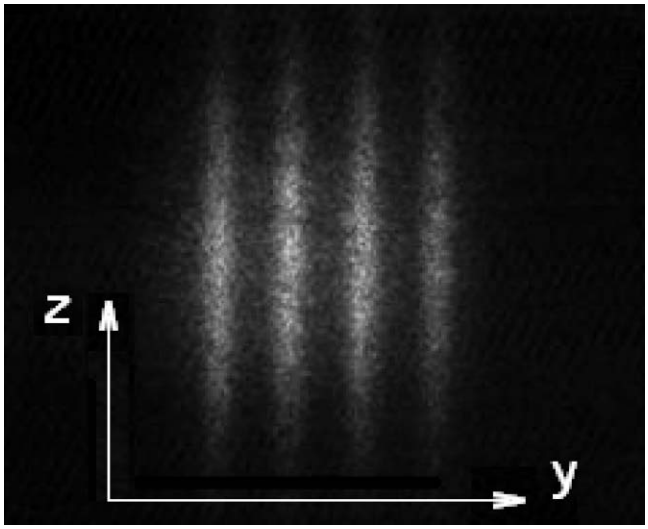

FIG. 4. Contour holographic interferogram of the tilted metallic plate for four laser modes and $\lambda_S = 6.6284$ mm.

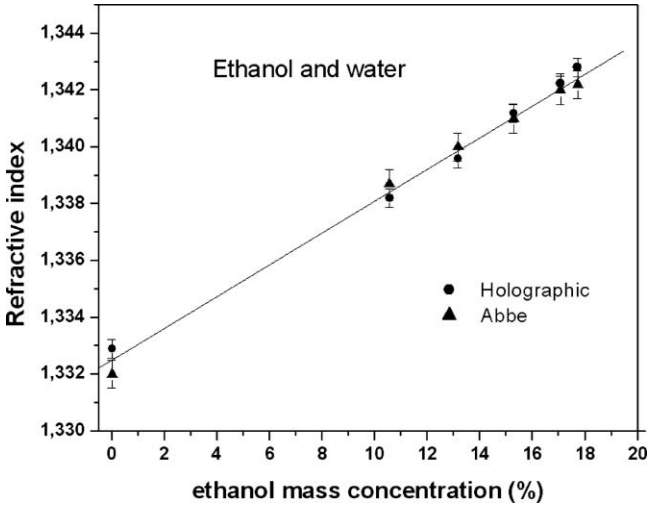

FIG. 5. Refractive index of the mixture ethanol + water as a function of the ethanol mass fraction, measured with the holographic refractometer (circles) and by a commercial Abbe refractometer (triangles).

cooled or heated by a Peltier element. The prism reflector PR works immersed in the liquid and is supported by a mount from the top of the test cell, such that there is no mechanical contact between the PR mount and the cell walls. Through a step motor the 90°-prism is translated with a displacement resolution of 5 μm along the x-axis in a closed loop. Figure 3(c) shows the details of the PR mount and the test cell.

According to Eq. (1), the larger the number N of oscillating laser modes, the narrower the bright interference fringes.[22] It was also shown that the number of modes is strongly dependent on the laser drive current.[22,27] Hence, in order to determine the fringe order p most easily and precisely the laser current was selected in order to provide the narrowest possible bright fringes. Figure 4 shows the resulting holographic image of the tilted plate for an estimated number of $N = 4$ laser modes. Some measurements were also performed with the laser supplied by two 1.5-V, AA batteries. As the PR is displaced, one observes the fringes running on the holographic image. The synthetic wavelength was then determined by translating the reflector PR by $\Delta L_1 = 69.595 \pm 0.005$ mm in an empty test cell to achieve a displacement of $p_1 = 21$ fringes with respect to a reference point on the object, resulting in a synthetic wavelength of $\lambda_S = 2\,\Delta L_1 / p_1 = 6.6280 \pm 0.0005$ mm.

A. Refractive index of water/ethanol mixture

By illuminating the interferometer with a single multimode laser as shown in Fig. 2 the refractive index of water with different concentrations of ethanol was measured. Since the maximum translation of the PR in the test cell was ~70 mm, for each concentration a typical procedure consisted of measuring the value of ΔL required for a displacement of $p = 28$ fringes. Figure 5 shows a plot of the refractive index of this mixture as a function of the ethanol mass fraction with respect to the whole liquid mass obtained through the holographic process (circles) and by a commercial Abbe refractometer (triangles). By comparing both measurements we obtained an average discrepancy below 0.05%, which can be considered satisfactory, since it is within the range of the uncertainty bars. This difference cannot be attributed to systematic measurement errors or to temperature phenomena, since for some concentrations the results obtained through the holographic method are larger, and for other concentrations, smaller.

B. Refractive index of NaCl aqueous solution

In this section we investigated the holographic refractometer performance concerning one of the most important applications of refractometry, i.e., the determination of a solute concentration in a solution by comparing its refractive index with a standard result or curve. For this study we determined the NaCl concentrations of five different solutions by measuring their refractive indexes and using an equation obtained in reference.[28] This empiric polynomial expression for the refractive index n_S has seven terms relating the solution refractive index with the temperature T and the NaCl concentration C_S. Following our experimental parameters we set the room temperature $T = 20.5$ °C so that C_S is obtained from this formula as

$$C_S = \frac{n_S - n_0}{\kappa}, \tag{4}$$

where $n_0 = 1.332\,14 \pm 0.000\,04$ and $\kappa = 0.1768 \pm 0.0008$ ml/mg, and C_S is given in units of mg of solute by milliliters of water. Figure 6 shows the refractive indexes for the holographic refractometer (circles) and the Abbe refractometer (triangles) compared with their expected values (solid line), while the results for the NaCl concentrations obtained from Eq. (4) for both devices are listed in Table I. This table compares the previously known NaCl concentrations—C_{SNaCl}, listed in the first column—with the results obtained through the holographic (C_{SH}) and the Abbe (C_{SA}) refractometers, as shown in the third and sixth columns, respectively. The concentrations C_{SH} and C_{SA} were obtained with the help of

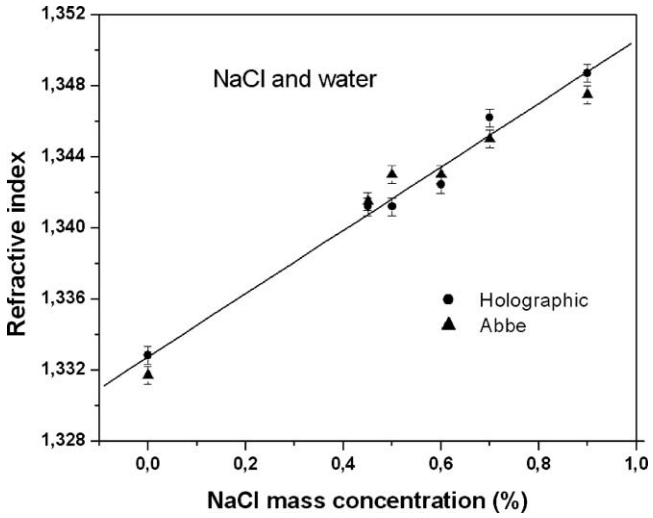

FIG. 6. Refractive index of the aqueous NaCl solution vs the NaCl concentration, measured with the holographic refractometer (circles) and with the Abbe refractometer (triangles). The solid curve refers as to the data obtained from Eq. (4).

Eq. (4), by using the refractive indexes n_{SH} and n_{SA} (shown in the second and fifth columns, respectively) measured through the holographic and the Abbe refractometers. The percent errors δ_H and δ_A calculated through the expression $\delta_{H,A} = 100 \times |C_S - C_{SH,A}|/C_{SNaCl}/C_{SNaCl}$ provide the accuracy of both methods: they presented an average value of 7% for the holographic method and of 10% for the Abbe refractometer.

C. Two-laser holographic refractometry

In order to perform two-laser holographic refractometry a small change in the holographic setup was introduced, as shown in Fig. 7. The beams coming from the tunable diode lasers 1 and 2 are spatially coupled by beam splitter BS. After BS the collinearly propagating beams illuminate the whole arrangement as in the one-laser setup. More details about two-laser holographic setups can be found elsewhere.[25,29] Both lasers are of the same model with emission wavelength centered at ~662 nm. By properly selecting the currents in the drivers the lasers were tuned in order to provide the synthetic wavelength $\lambda_S = 788.8 \pm 0.3$ μm, which corresponds to a wavelength difference of $\lambda_1 - \lambda_2 = 0.56$ nm. The synthetic wavelength was determined by adopting the same procedure as in Sec. III.

TABLE I. Measurement of NaCl concentrations in an aqueous solution by refractometry. C_{SNaCl} are the known concentrations (first column) and C_{SH} (third column) and C_{SA} (sixth column) are the NaCl concentrations obtained through the holographic and the Abbe refractometers, respectively.

	Holographic			Abbe		
C_{SNaCl} (10^{-2} g/ml)	n_{SH}	C_{SH} (10^2 g/ml)	δ_H(%)	n_S	C_{SA} (g/kg)	δ_A(%)
4.5	1.3412	5.107	13.5	1.3415	5.294	17.6
5.0	1.3412	5.107	2.1	1.3430	6.142	22.8
6.0	1.3424	5.813	3.1	1.3430	6.142	2.4
7.0	1.3462	7.934	13.3	1.3450	7.293	4.2
9.0	1.3486	9.360	4.0	1.3475	8.687	3.5

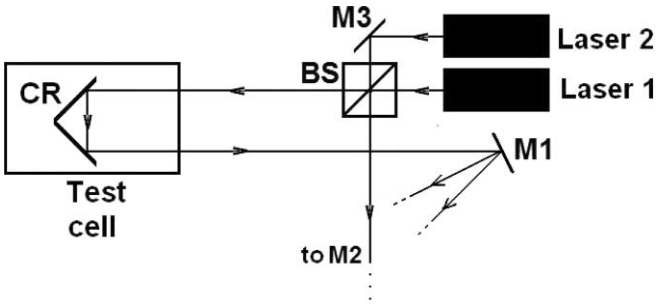

FIG. 7. Optical arrangement for two-laser holographic refractometry.

An amount of 20 ml of artificial melon juice at 10 °C was introduced into the test cell. Actually, the amount sufficient for the measurement is much smaller (about 1 ml or less), but the test cell was not optimized for this case. After translating the 90°-prism reflector by 5.33 ± 0.01 mm one observed the displacement of 18 fringes, resulting in a refractive index of 1.331 ± 0.002, according to Eq. (3). Figure 8 shows the clearly visible contour fringes on the holographic image of the metallic plate despite the losses on the reference beam due to the turbid liquid when the liquid column was ~6 mm. Concerning phenomena like scattering and absorption, the total loss on the reference beam was 7.5%, corresponding to a loss coefficient for red light of $\alpha \approx 0.13$ cm^{-1}, according to Beer´s law. This result shows that working with smaller synthetic wavelengths is of crucial importance in the analysis of highly scattering or absorbing liquids, since in this case smaller liquid column lengths are required; on the other hand, with the single-laser holographic setups described in the previous sections and their relatively large synthetic wavelengths, the liquid column lengths must be of the order of tens of millimeters in order to increase the measurement sensitivity and accuracy, but in this case the losses would dramatically increase to ~60%, which would make the holographic recording unviable or spoil the fringe visibility.

IV. DISCUSSION

Comparing with other techniques, the most distinguishing properties of the holographic refractometry technique presented in this paper are the wide range of measurable

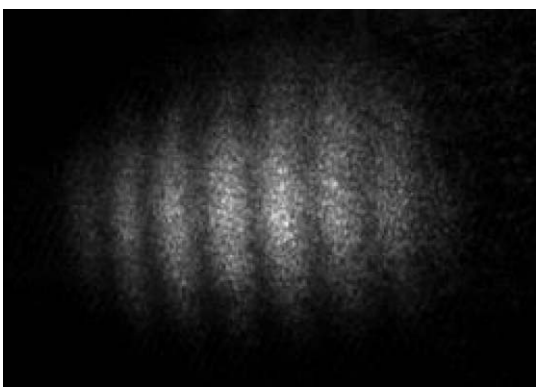

FIG. 8. Two-laser holographic interferogram of the flat object for $\lambda_S = 788.8 \pm 0.5$ μm.

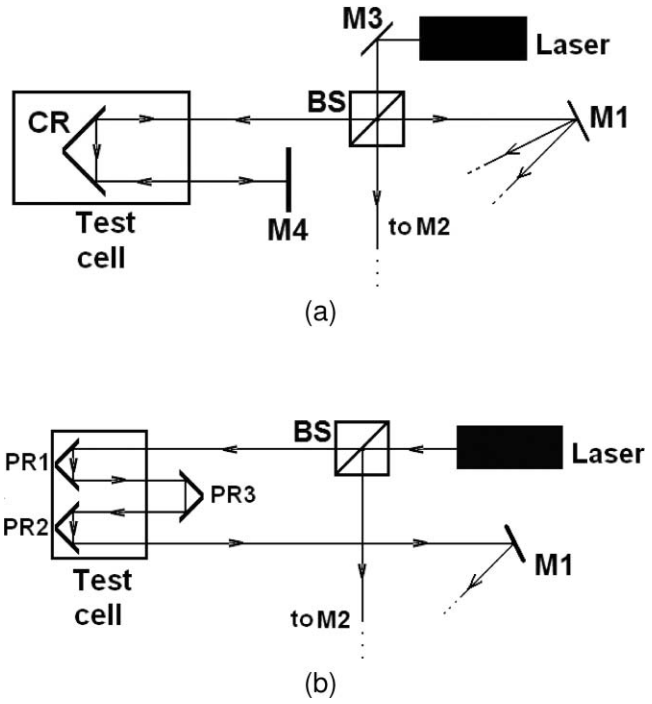

FIG. 9. (a) and (b) Optical schemes on the reference-beam arm for effective ΔL enlargement. M3 and M4, mirrors, PR1, PR2, and PR3, 90°-prisms.

refractive index values and the scalable measurement precision. The first is due to the fact that the measurement does not depend on the refractive indexes of the media surrounding the liquid analyzed; the latter can be justified with the help of the refractive index uncertainty obtained from Eq. (3):

$$\delta n = n\left\{\left(\frac{\delta\lambda_S}{\lambda_S}\right)^2 + \left(\frac{\delta(\Delta L)}{\Delta L}\right)^2\right\}^{1/2}, \tag{5}$$

where $\delta(\Delta L) = 0.005$ mm is the precision of the micrometric translation stage while the synthetic wavelength uncertainty is given by $\delta\lambda_S = 0.0005$ mm. Equation (5) shows clearly that the larger the path ΔL through the liquid, the smaller the uncertainty δn. By taking advantage from this characteristic we tested other reflector geometries in the test cell in order to increase the precision and enhance the measurement sensitivity without significantly enlarging the liquid amount. Figure 9 shows two examples of employ of right angle prisms in the reference-beam arm. The arrangement shown in Fig. 9(a) uses a mirror M4 for doubling the light path inside the cell: the beam reflected by the beam splitter passes through the test cell, hits mirror M4, and propagates through the cell once more. Thus, the beam optical path inside the cell is twice the one of Fig. 1. In Fig. 9(b) the setup uses two prisms PR1 and PR2 inside the cell and an external one PR3 in order to provide the same result. The figure clearly shows that the additional prisms PR2 and PR3 double the optical path through the liquid. The first configuration is simpler and requires less amounts of liquid if compared to the latter but introduces more losses since the reference beam bounces twice in the beam splitter, which leads to a longer hologram buildup time or to a decrease in the diffracted light intensity. The examples shown in Fig. 9 may suggest many other prism and mirror combinations in order to scale to higher precisions.

The simplicity of Eq. (3) leads to few uncertainty sources, as well as the simple optical setup and measurement method favor the appearing of only a few error sources. This can be mainly attributed to the positioning of the test cell in the reference-beam arm of the interferometer. The small diameter (<3 mm) of the beam impinging the cell makes the requirements for flatness and thickness uniformity of the front cell window to be somewhat relaxed. In fact, in our setup simple, low-cost microscope glasses were used as cell windows. The errors caused by an eventual deformation of the reference beam wavefront become even more negligible by taking into account that the size of the object image is significantly smaller than the reference beam cross section when they overlap at the BTO crystal.

The systematic measurement errors are mostly due to misalignments on the liquid cell and the reflectors. A small and undesirable angle γ between the direction of the beam inciding onto the test cel and the translation direction of the reflector PR causes an error on the refractive index given by $\Delta n \approx n\gamma^2/2$. A small deviation angle α from normal incidende of the same beam on the front window of the test cell leads to an error $\Delta n' \approx \alpha^2/(2n)$. Depending upon how the system is aligned both effects can whether reinforce (i.e., increase) or even cancel each other.

V. CONCLUSIONS

The development of a portable holographic refractometer prototype for liquid analysis based on multiwavelength photorefractive holography was described, and its performance was analyzed. The test cell was inserted into the reference-beam arm, and a flat metallic bar was utilized as the object whose contour fringes were generated due to the multiwavelength holographic recording. As the reflector was translated the straight and parallel fringes run over a reference point on the object thus enabling the refractive index determination. According to Eq. (3) the change of one fringe order ($\Delta p = 1$) requires a $\lambda_S/2$-reflector displacement. Hence, since the synthetic wavelengths generated in the holographic processes are much larger than the micrometric screw precision, the fringe order could be accurately and precisely determined. Moreover, the relatively large synthetic wavelengths does enable utilizing simple, easily available translation stages moved manually or by cost-effective step motors. The imaging of the contour fringe pattern on a CCD sensor instead of the signal detection through a small-area photodetector contributed to an easy visual determination of the fringe position, enabling measurements even in moderately unstable holographic recordings. The refractive index measurement of turbid liquids was also successfully demonstrated through two-laser holography, providing a synthetic wavelength of 788.8 μm and enabling the measurement of a liquid with a loss coefficient of 0.13 cm^{-1}.

The results obtained through the holographic method have shown to be very accurate upon comparison with the Abbe refractometer data. This accuracy and the precision of the method can be further improved by exploring its flexibility

characteristics without radically changing the whole apparatus, e.g., by enlarging the effective liquid column—with the expense of larger liquid quantities—or by using a setup with two diode lasers.

ACKNOWLEDGMENTS

This work was partially supported by the Conselho Nacional Científico e Tecnológico (CNPq) under Grant No. 473458/2006-3 and by the Fundação de Apoio à Tecnologia. D. M. S. was sponsored by an undergraduate scholarship from CNPq.

[1] M. Riche, Aquaculture **264**, 279 (2007).
[2] C. Cray, M. Rodriguez, and K. L. Arheart, Vet. Clin. Pathol. **37**, 438 (2008).
[3] C. Bertucci, S. Cimitan, L. Menotti, C. Bertucci, S. Cimitan, and L. Menotti, J. Pharm. Biomed. Anal. **32**, 697 (2003).
[4] M. D. Green, H. Nettey, O. V. Rojas, C. Pamanivong, L. Khounsaknalath, M. G. Ortiz, P. N. Newton, F. M. Fernández, L. Vongsack, and O. Manolin, J. Pharm. Biomed. Anal. **43**, 105 (2007).
[5] K. Zirk and H. Poetzschke, Med. Eng. Phys. **26**, 473 (2004).
[6] K. Zirk and H. Poetzschke, Med. Eng. Phys. **29**, 449 (2007).
[7] A. M. Zysk, E. J. Chaney, and S. A. Boppart, Phys. Med. Biol. **51**, 2165 (2006).
[8] F. Onofri, M. Krysiek, and J. Mroczka, Opt. Lett. **32**, 2070 (2007).
[9] A. S. Andrushchak, B. V. Tybinka, I. P. Ostrovskij, W. Schranz, and A. V. Kityk, Opt. Lasers Eng. **46**, 162 (2008).
[10] G. H. Meeten and P. Navard, Polymer **23**, 483 (1982).
[11] M. B. Huglin and R. W. Richards, Polymer **17**, 587 (1976).
[12] N. Bauer, K. Fajans, and S. Z. Lewin, in *Physical Methods of Organic Chemistry*, edited by A. Weissberger (Interscience Publishers, New York, 1960), Vol. I.
[13] L. W. Tilton and J. K. Taylor, in *Physical Methods in Chemical Analysis*, edited by W. G. Berl (Academic, New York, 1960), Vol. I.
[14] E. Abbe, *Neue Apparate zur Bestimmung des Brechungs–und Zerstreuungsvermöfester und flüssiger Körper* (Mauke's Verlag, Jena, 1874).
[15] D. W. Kim, Y. Zhang, K. L. Cooper, and A. Wang, Appl. Opt. **44**, 5368 (2005).
[16] P. H. Tomlins, P. Woolliams, C. Hart, A. Beaumont, and M. Tebaldi, Opt. Lett. **33**, 2272 (2008).
[17] D. W. Kim, F. Shen, X. Chen, and A. Wang, Opt. Lett. **30**, 3000 (2005).
[18] P. Dumais, C. L. Callender, J. P. Noad, and C. J. Ledderhof, Opt. Exp. **16**, 27 (2008).
[19] M. de Angelis, S. De Nicola, P. Ferraro, A. Finizio, and G. Pierattini, Pure Appl. Opt. **5**, 761 (1996).
[20] D. H. McQueen, J. Phys. E **12**, 111 (1979).
[21] M. Gustafsson and M. Sebesta, Appl. Opt. **43**, 4796 (2004).
[22] E. A. Barbosa, R. Verzini, and J. F. Carvalho, Opt. Commun. **263**, 189 (2006).
[23] C. M. Vest, *Holographic Interferometry* (Wiley, New York, 1979).
[24] E. A. Barbosa, Appl. Phys. B: Lasers Opt. **80**, 345 (2005).
[25] E. A. Barbosa and J. F. Carvalho, Appl. Phys. B: Lasers Opt. **87**, 417 (2007).
[26] A. A. Kamshilin and M. P. Petrov, Opt. Commun. **53**, 23 (1985).
[27] E. A. Barbosa, E. A. Lima, M. R. R. Gesualdi, and M. Muramatsu, Opt. Eng. **46**, 075601 (2007).
[28] R. B. Santiago Neto, J. P. R. F. de Mendonça, and B. Lesche, Rev. Fis. Apl. e Inst. **17**, 74 (2004).
[29] E. A. Barbosa, Opt. Express **18**, 8743 (2010).